Geomechanics and Engineering, *Vol. 37, No. 4 (2024) 323-339*
https://doi.org/10.12989/gae.2024.37.4.323

Blow-out pressure of tunnels excavated in Hoek-Brown rock masses

Alireza Seghateh Mojtahedi[1a], Meysam Imani*[2] and Ahmad Fahimifar[1b]

[1]*Department of Civil and Environmental Engineering, Amirkabir University of Technology, Tehran, Iran*
[2]*Garmsar Campus, Amirkabir University of Technology, Garmsar, Iran*

(*Received December 7, 2022, Revised September 17, 2023, Accepted April 25, 2024*)

Abstract. If the pressure exerted on the face of a tunnel excavated by TBM exceeds a threshold, it leads to failure of the soil or rock masses ahead of the tunnel face, which results in heaving the ground surface. In the current research, the upper bound method of limit analysis was employed to calculate the blow-out pressure of tunnels excavated in rock masses obeying the Hoek-Brown nonlinear criterion. The results of the proposed method were compared with three-dimensional finite element models, as well as the available methods in the literature. The results show that when σ_{ci}, m_i, and GSI increase, the blow-out pressure increases as well. By doubling the tunnel diameter, the blow-out pressure reduces up to 54.6%. Also, by doubling the height of the tunnel cover and the surcharge pressure exerted on the ground surface above the tunnel, the blow-out pressure increased up to 74.9% and 5.4%, respectively. With 35% increase in the unit weight of the rock mass surrounding the tunnel, the blow-out pressure increases in the range of 14.8% to 19.6%. The results of the present study were provided in simple design graphs that can easily be used in practical applications in order to obtain the blow-out pressure.

Keywords: blow-out; Hoek-Brown; rock masses; tunnel; upper-bound method

1. Introduction

A major issue in mechanized tunneling is to maintain the stability of the tunnel face by keeping the face pressure within a specific range. If the face pressure becomes smaller than the magnitude required for stability, an active failure occurs in which the tunnel face collapses toward the tunnel. If the face pressure becomes larger than a critical magnitude, the soil/rock masses ahead of the tunnel will experience passive failure, which results in heaving the ground above the tunnel face. This critical passive pressure is known as the blow-out pressure.

Various experimental, numerical, and analytical methods were proposed by researchers to determine the tunnel face pressure corresponding to the active failure state. Most of these methods are related to soil grounds, considering the Mohr-Coulomb failure criterion. Among others, one can mention the investigations conducted by Broms and Bennermark (1967), Horn (1961), Murayama *et al.* (1966), Leca and Dormieux (1990), Davis *et al.* (1980), Anangnostou and Kovari (1994), Jancsecz and Steiner (1994), Sloan and Assadi (1994), Mair and Taylor (1997), Broere (2001), Herrenknecht and Rehm (2002), Vermeer *et al.* (2002), Guglielmetti *et al*. (2008), Kirsch *et al*. (2009), Mollon *et al.* (2009a, b), Mollon *et al*. (2010), Mollon *et al*. (2011a, b), Anagnostou (2012), Mollon *et al.* (2013), Han *et al.* (2016), Khezri *et al*. (2016), Zhang *et al*. (2015), Pan and Dias (2017), Zhao *et al*. (2017), Zamora Hernández *et al.* (2019), Zou *et al.* (2019), Li *et al*. (2020), Li *et al*. (2022) and Yang *et al*. (2022). Additionally, few studies are available regarding the active face pressure in rocky grounds (Senet *et al.* 2013, Pan and Dias 2018, Li and Yang 2019, Huang *et al.* 2019, Seghateh Mojtahedi *et al*. 2021).

Given the difficulty of constructing physical models for determining the blow-out pressure, this method was rarely employed by researchers. Among others, Bezuijen and Brassinga (2006) and Wong *et al.* (2012) employed centrifuge tests to determine the blow-out pressure in sandy soils. Moreover, Berthoz *et al.* (2012) investigated the blow-out pressure by constructing several 1g models. As another research tool, numerical methods were suitably used by some other researchers, including the investigations performed by Subrin (2002), Mollon *et al*. (2013), and Huang *et al.* (2018) using the finite difference method (FDM) and that performed by Shiau and Al-Asadi (2020) using 3D finite element limit analysis (FELA). Along with numerical methods, analytical methods play a major role in solving tunnel stability problems due to easily implementing their results in practical problems. Leca and Dormieux (1990) proposed a two-block failure mechanism to determine the blow-out pressure of a tunnel face constructed in soil. This mechanism was later extended to a multi-block failure mechanism by Mollon *et al.* (2009a). Also, Mollon *et al*. (2011a) applied the upper bound method to study the blow-out pressure in frictional soils using a three-dimensional rotational failure mechanism. This mechanism was subsequently extended by Mollon *et al*. (2013) to determine the blow-out pressure in saturated cohesive soils. The multi-block mechanism proposed by Mollon *et al.* (2009a) constituted a basis for later research

*Corresponding author, Assistant Professor
E-mail: imani@aut.ac.ir
[a]Ph.D. Candidate
E-mail: mojtahedi@aut.ac.ir
[b]Professor
E-mail: fahim@aut.ac.ir

ISSN: 2005-307X (Print), 2092-6219 (Online)

and was extended by Zhao *et al.* (2017) and Li *et al.* (2020) for a longitudinally inclined tunnel and tunneling in sloping grounds, respectively. Furthermore, Li *et al*. (2019) used the aforementioned mechanism for determining the blow-out pressure in sandy soils. Also, Huang *et al.* (2021) studied blow-out failure mechanism of tunnels excavated in soils subjected to groundwater using upper bound theorem.

A literature review reveals that very few research works were conducted to determine the blow-out pressure in rock masses. The equations used for obtaining the blow-out pressure in soils are typically based on Mohr-Coulomb failure criterion and cannot produce sufficient accuracy in rock masses since the Hoek-Brown failure criterion is more common in rock masses. To the authors' knowledge, the major contribution regarding the blow-out pressure in rock masses was performed by Huang *et al*. (2018). Based on the upper bound method, they applied a two-dimensional failure mechanism, which cannot represent the three-dimensional behavior of the blow-out pressure. Moreover, Huang *et al.* (2018) focused on the final shape of the blow-out failure mechanism corresponding to a known blow-out pressure, while the major concern of tunnel designers is the value of the blow-out pressure, not just the shape of the failure mechanism.

The present paper introduces an upper bound solution to determine the blow-out pressure in weak rock masses. A three-dimensional multi-block failure mechanism was proposed to consider different internal friction angles in different sliding blocks of the failure mechanism. Therefore, the proposed failure mechanism is more elaborated than most previous mechanisms and significantly improves the accuracy of the blow-out pressure. The results obtained from the proposed upper bound technique were compared with three-dimensional finite element models. The effects of the tunnel diameter, the height of the tunnel cover, the unit weight of the rock mass surrounding the tunnel, and the surcharge pressure exerted to the ground surface on the blow-out pressure were also studied.

2. The proposed failure mechanism

2.1 Hoek-Brown failure criterion

This study employed the modified nonlinear Hoek-Brown failure criterion (2002), i.e., Eq. (1), for the rock mass surrounding the tunnel.

$$\sigma_1' = \sigma_3' + \sigma_{ci}(m_b \frac{\sigma_3'}{\sigma_{ci}} + s)^a \quad (1)$$

In which, m_b, s, and a can be obtained as follows

$$m_b = m_i \exp(\frac{GSI-100}{28-14D}) \quad (2)$$

$$s = \exp(\frac{GSI-100}{9-3D}) \quad (3)$$

$$a = \frac{1}{2} + \frac{1}{6}\left[\exp\left(-\frac{GSI}{15}\right) - \exp\left(-\frac{20}{3}\right)\right] \quad (4)$$

The parameters of the above equations were defined in the Symbols list. This nonlinear failure criterion is usually linearized to be applied in the upper bound limit analysis. Two common approaches are existed for linearization, which includes the single-tangential line method (Yang and Yin 2005, Saada *et al*. 2008, 2012, Imani and Aali 2020) and the multi-tangential line method (Mao *et al.* 2012, Senet *et al*. 2013, Seghateh Mojtahedi *et al*. 2021). In the single-tangential line method, the Hoek-Brown nonlinear criterion is replaced by a single straight line whose inclination, i.e., the equivalent internal friction angle ϕ_t, is obtained via optimization. Afterwards, the corresponding equivalent cohesion c_t is determined using Eq. (5) proposed by Yang and Yin (2005).

$$\frac{c_t}{\sigma_{ci}} = \frac{\cos\phi_t}{2}\left[\frac{m_b\, a\,(1-\sin\phi_t)}{2\sin\phi_t}\right]^{\frac{a}{1-a}} - \frac{\tan\phi_t}{m_b}\left(1 + \frac{\sin\phi_t}{a}\right)\left[\frac{m_b\, a\,(1-\sin\phi_t)}{2\sin\phi_t}\right]^{\frac{1}{1-a}} + \frac{s}{m_b}\tan\phi_t \quad (5)$$

In the single-tangential line approach, the obtained values of ϕ_t and c_t should be assigned to the whole failure mechanism. It is clear that having constant ϕ_t and c_t magnitudes is not compatible with the nature of rock mass. This limitation was overcome by using the multi-tangential linearization technique shown in Fig. 1. In this method, the nonlinear criterion is replaced by several tangent lines, each one has a unique ϕ_t and c_t, so the accuracy of the results improves significantly compared with the single-tangential line technique. The value of each ϕ_t and the corresponding c_t are obtained similar to the procedure explained for the single-tangential line method. This technique was previously used for determining the bearing capacity of rock masses (Mao *et al.* 2012, AlKhafaji *et al*. 2020, Shamloo and Imani 2021), tunnel face pressure (Senet *et al.* 2013, Seghateh Mojtahedi *et al*. 2021), and it was used for obtaining the blow-out pressure of tunnels in the present paper.

2.2 The formation of sliding blocks in the proposed failure mechanism

The failure mechanism proposed in this study consists of several rigid sliding blocks, each of them moves at a specific velocity. The angle between each of the velocity vectors and the corresponding discontinuity surface is equal to ϕ_t (Chen 1975). Therefore, since the present research used the multi-tangential technique leading to several ϕ_t values in the mechanism, the angle between each velocity vector and the corresponding discontinuity surface is unique. The general shape of the 3D failure mechanism proposed in the present paper is shown in Fig. 2. The mechanism comprises several sliding blocks ($AB_{i-1}B_i$: i=1 to n-1) and a sliding block touching the ground surface (the truncated cone $AEFB_n$).

In the previous researches, which were based on the existence of a constant friction angle in the whole mechanism, each sliding block in the mechanism was formed based on the geometry of its previous sliding block. However, in the failure mechanism proposed herein, because of variation of the friction angle in different blocks, producing a sliding block from its previous block is no

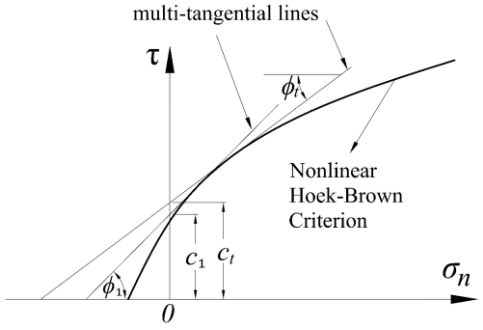

Fig. 1 The multi-tangential linearization of the Hoek-Brown nonlinear criterion

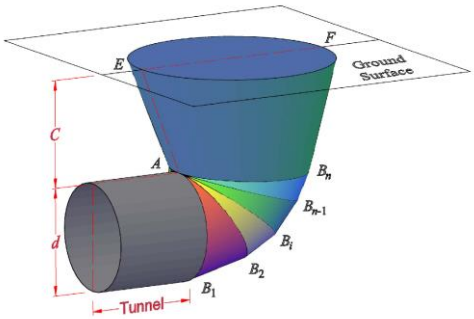

Fig. 2 General view of the proposed failure mechanism

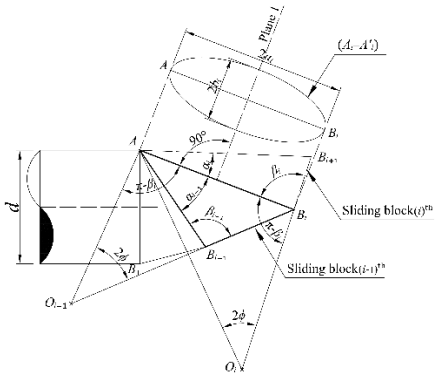

Fig. 3 The generation of sliding blocks in the failure mechanism proposed by Mollon *et al.* (2009a) and Zhao *et al*. (2017)

longer possible. For a better understanding of this concept, one may refer to the failure mechanisms proposed by Mollon *et al.* (2009a) and Zhao *et al.* (2017), as shown in Fig. 3. In this mechanism, a single constant ϕ was considered throughout the mechanism, resulting in the vertex angle $AO_{i\text{-}1}B_{i\text{-}1}$ equal to 2ϕ. This mechanism cannot be used in the present research since different values of ϕ_t were considered in the present study, not a single unique one. Seghateh Mojtahedi *et al.* (2021) developed a new failure mechanism for determining the face pressure of tunnels in rock masses (active failure) which can consider various ϕ_t values. However, the same idea was applied here, but it was revised to cover the blow-out pressure (passive failure).

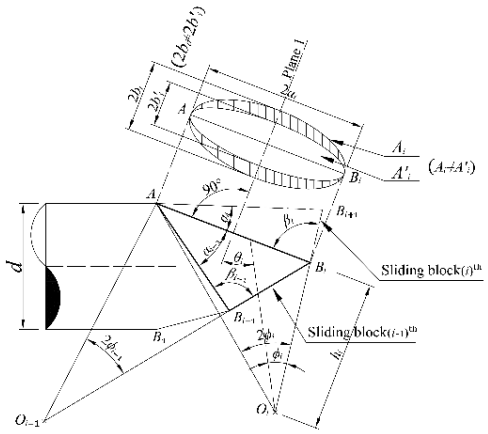

Fig. 4 The generation of sliding blocks in the proposed failure mechanism

Fig. 4 displays the generation method of the sliding blocks of the failure mechanism proposed in the current work. The vertex angle of each cone AO_iB_i is unique and is equal to $2\phi_i$, and the area of the cone elliptical-shaped cross-section is equal to A_i, with the major and minor diameters of $2a_i$, and $2b_i$, respectively. The cross-sectional area of each new cone was obtained by symmetrizing the extended cone $AO_{i\text{-}1}B_i$ with respect to the perpendicular bisector exerted to the plane AB_i (i.e., Plane 1) which is an ellipse with the area equal to A'_i, and the major and minor diameters equal to $2a_i$, and $2b'_i$, respectively. The innovation of the presented mechanism is that the minor diameters and also the areas of these ellipses on the AB_i plane are different ($2b_i \neq 2b'_i$ and $A_i \neq A'_i$) since the vertex angles of the adjacent cones are not the same ($\widehat{AO_{i\text{-}1}B_{i\text{-}1}} \neq \widehat{AO_iB_i}$). Hence, despite increasing the number of variables, constraints, and complexities of the obtained upper bound relationships, more accurate results were obtained from the proposed mechanism. This method of producing each sliding block is more elaborate than the methods used by Mollon *et al.* (2009a), and Zhao *et al.* (2017), in which a constant ϕ angle was considered throughout the whole mechanism resulting in each sliding block having the same vertex angle, i.e., $2\phi_{i\text{-}1}$, as its previous block $AO_{i\text{-}1}B_{i\text{-}1}$. In other words, in the mentioned methods the ellipses on the AB_i plane were exactly the same ($2b_i = 2b'_i$ and $A_i = A'_i$).

2.3 The configuration of the proposed failure mechanism

Fig. 5 displays a longitudinal cross-section of the proposed failure mechanism. The velocity field of the mechanism and the corresponding hodograph are shown in Figs. 6(a) and 6(b), respectively. The velocity of each sliding block and the relative velocity between two successive sliding blocks were shown by U_i and $U_{i,i+1}$, respectively. The angle between each velocity vector (U_i or $U_{i,i+1}$) and the surface on which it applies is equal to the tangential friction angle ϕ_t, which is unique for every velocity discontinuity surface throughout the mechanism ($\phi_i \neq \phi_{i+1} \neq \phi_{i,i+1}$). As discussed earlier, the value of these

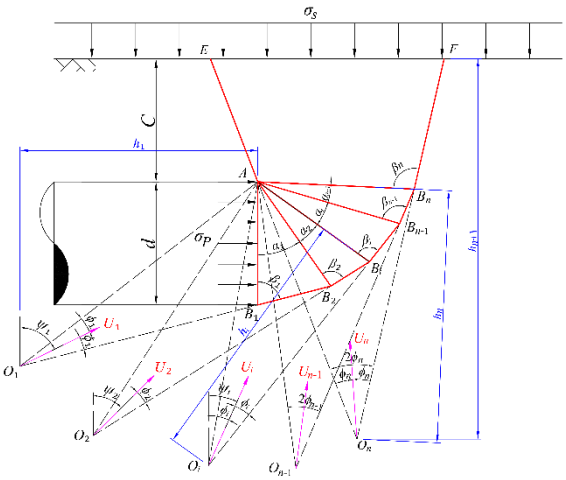

Fig. 5 The longitudinal cross section of the proposed failure mechanism

tangential friction angles is unknown and should be determined through optimization. All the geometric relationships of the sliding blocks and the velocity vectors are presented in detail in the Appendix.

3. Calculation of the blow-out pressure

3.1 External work

The total external work exerted on the mechanism (W) was obtained by adding up the external works due to the weight of the sliding blocks (W_γ), the pressure applied to the tunnel face (W_p), and the surcharge applied to the ground surface (W_s) as follows

$$W = W_\gamma + W_p + W_s \tag{6}$$

Where

$$W_\gamma = -\gamma\left[\sum_{i=1}^{n-1}(V_i U_i \cos\psi_i) + V_{TC} U_n \cos\psi_n\right] \tag{7}$$

$$W_p = \sigma_p A_1 U_1 \sin\psi_1 = \sigma_p A_1 U_1 \sin(\beta_1 - \phi_1) \tag{8}$$

$$W_s = -\sigma_s A_{n+1} U_n \cos\psi_n \tag{9}$$

The parameters used in the abovementioned equations were defined in the Symbols list. According to Eq. (7), the external work depends on the volume of the sliding blocks

For example, a block of volume V_i is shown in Fig. 7(a). For calculating the volume of this block, a local coordinate system centered at A (0,0) was considered in such a way that its X and Y-axes lie along the major and minor diameters of the $(i+1)^{th}$ elliptical cross-section, respectively (see Fig. 7(b)). A volume element with a cross-section of $efgh$ and a thickness of Δx_{i+1} along the local X-axis was considered in the space between the i^{th} and $(i+1)^{th}$ elliptical cross-sections and parallel to B_iB_{i+1} line (see Fig. 7(c)). By integrating this volume element within the interval of 0 to $2a_{i+1}$, the volume of the block was obtained as denoted in

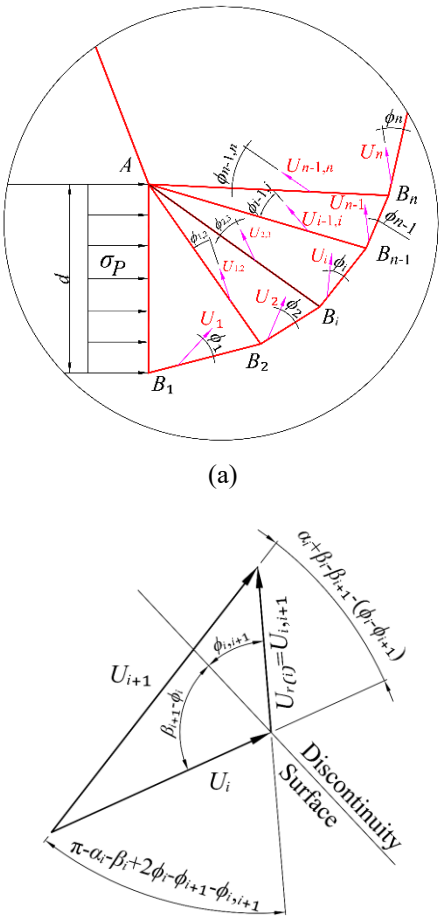

(a)

(b)

Fig. 6 (a) The velocity field of the proposed failure mechanism and (b) the corresponding hodograph

Eq. (A-18) of the Appendix. The volume of all sliding blocks in the mechanism, except for the last one reaching the ground surface, can be calculated similarly. The volume of the last block (the truncated cone $AEFB_n$ in Fig. 2) can be computed using Eq. (A-31) of the Appendix.

3.2 Internal energy dissipation

The total internal energy dissipated in the mechanism (D) was determined by adding up the energies dissipated over the external surfaces of the sliding blocks (D_S) and at the interface of two successive sliding blocks (D_A) as follows

$$D = D_s + D_A \tag{10}$$

Where

$$D_S = \sum_{i=1}^{n-1}\left(c_i U_i S_i \int_0^{2a_{i+1}} \cos\delta_i \, dx_{i+1} \cdot \cos\phi_i\right) + c_n U_n S_{TC} \cos\phi_n \tag{11}$$

$$D_A = \sum_{i=1}^{n-1}(c_{i,i+1} U_{i,i+1} A_{i+1} \cos\phi_{i,i+1}) \tag{12}$$

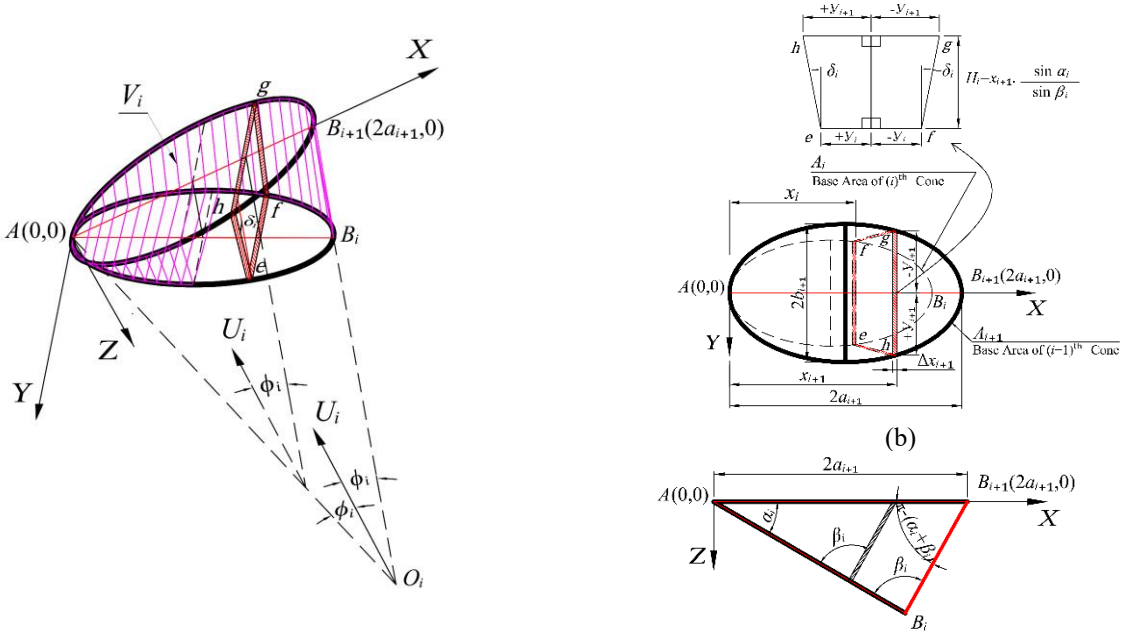

Fig. 7 The procedure of computing the volume of the sliding blocks: (a) The volume of the i^{th} sliding block, (b) the *X*-*Y* view, and (c) the *X*-*Z* view

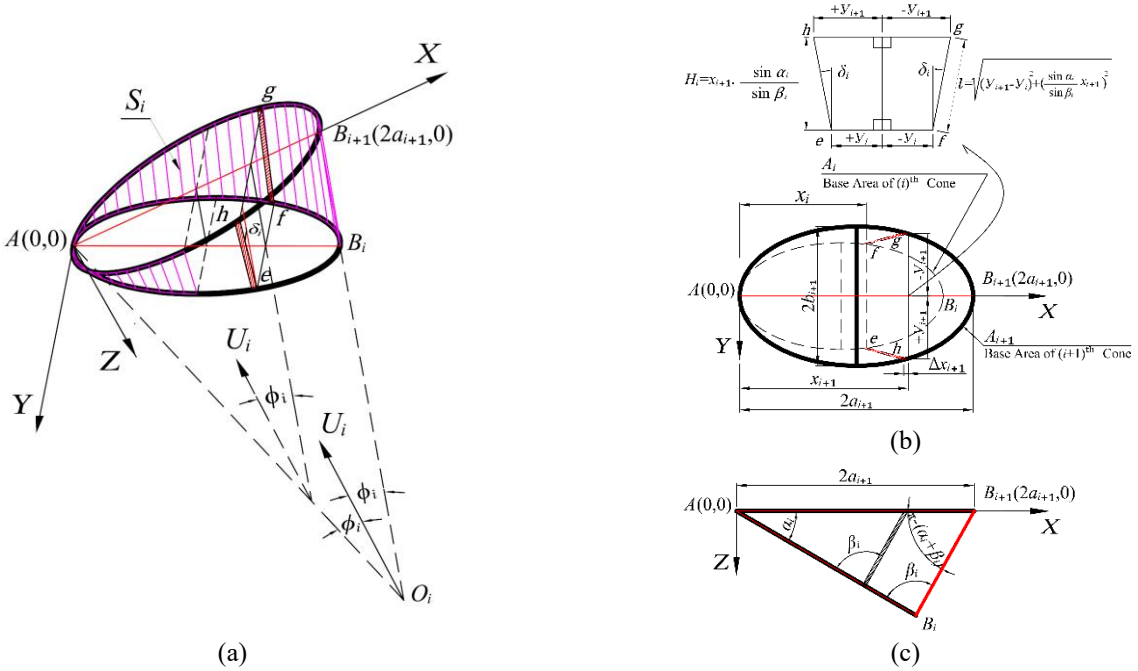

Fig. 8 The procedure of computing the surface of the sliding blocks: (a) The lateral surface of the i^{th} sliding block, (b) the *X*-*Y* view, and (c) the *X*-*Z* view

The parameters used in the abovementioned equations were defined in the Symbols list. According to Eqs. (11) and (12), it is clear that calculating the area of various surfaces of the sliding blocks is required to determine the internal energy dissipated in the mechanism. For example, the calculation procedure of the area of the surfaces that existed in the sliding blocks is shown in Fig. 8(a). A local coordinate system centered at *A* (0,0) was defined in such a way that its *X* and *Y*-axes lie along the major and minor diameters of the $(i+1)^{th}$ elliptical cross-section, respectively (see Fig. 8(b)). The surface element ds_{ai} with a length of *l* and a thickness of Δx_{i+1} was defined along the local *X*-axis, in the space between the i^{th} and $(i+1)^{th}$ elliptical cross-sections (see Fig. 8(c)). To calculate the lateral surface of the sliding block, the ds_{ai} element was integrated over the interval of 0 to $2a_{i+1}$ (according to Eq. (A-20) in the Appendix). Using such a routine, the area of all the required surfaces except for the lateral surface of the last block

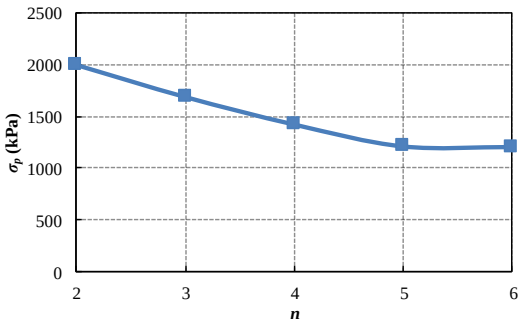

Fig. 9 Variation of σ_p versus n

reaching the ground surface was calculated. The lateral surface of the last block (the truncated cone $AEFB_n$ in Fig. 2) was calculated using Eq. (A-32) of the Appendix.

3.3 Blow-out pressure

According to the principle of virtual work, the external work performed in a failure mechanism is equal to the internal energy dissipated in the mechanism. Therefore, by equating Eqs. (6) and (10) and after some manipulations, the pressure applied to the tunnel face was obtained as follow

$$\sigma_p = \frac{\gamma \cdot [\sum_{i=1}^{n-1}(V_i U_i \cos\psi_i) + V_{TC} U_n \cos\psi_n] + \sigma_s A_{n+1} U_n \cos\psi_n + [\sum_{i=1}^{n-1}(c_i U_i S_i \int_0^{2\alpha_{i+1}} \cos\delta_i \, dx_{i+1} \cdot \cos\phi_i) + c_n U_n S_{TC} \cos\phi_n + \sum_{i=1}^{n-1}(c_{i,i+1} U_{i,i+1} A_{i+1} \cos\phi_{i,i+1})]}{A_1 U_1 \sin(\beta_1 - \phi_1)} \quad (13)$$

Where in its minimum possible magnitude, σ_p is the blow-out pressure. Therefore Eq. (13) should be optimized, i.e., minimized, in order to determine the blow-out pressure of tunnels excavated in rock masses.

3.4 Determining the optimized blow-out pressure

Eq. (13) contains some unknown parameters, namely α_i, β_i, ϕ_i, and $\phi_{i,i+1}$, which must be determined in such a way as to optimize (i.e., minimize) the σ_p. The optimization process was performed using the genetic algorithm provided in MATLAB software. For converging the optimization process to a proper answer and also for the final failure mechanism to be kinematically admissible, the following constraints were considered

$$\alpha_i + \beta_i > \beta_{i+1} \quad (14)$$

$$\alpha_i + \beta_i - \phi_i > \frac{\pi}{2} \quad (15)$$

$$\alpha_i + 2\beta_i > \pi \quad (16)$$

$$\sum_{i=1}^{n-1} \alpha_i < \beta_n - \phi_n \quad (17)$$

$$\alpha_i + \beta_i - \beta_{i+1} - \phi_i + \phi_{i+1} < \frac{\pi}{2} \quad (18)$$

$$\beta_i > 2\phi_i \quad (19)$$

$$\phi_{i+1} > \phi_i \quad (20)$$

$$\phi_{i+1,i+2} > \phi_{i,i+1} \quad (21)$$

$$0 < \alpha_i < \frac{\pi}{2} \quad (22)$$

$$0 < \beta_i < \pi \quad (23)$$

$$0 < \phi_i, \phi_{i,i+1} < \frac{\pi}{4} \quad (24)$$

3.5 The optimal number of sliding blocks in the failure mechanism

The number of unknown parameters and the precision of the optimization results depend on the number of sliding blocks (n) considered in the failure mechanism. If n exceeds an optimal number, the analysis time will increase significantly without any remarkable improvement in the solution accuracy. For obtaining the optimal number of sliding blocks, a tunnel with d=10 m and C=10 m was considered in a rock mass with σ_{ci}=1 MPa, m_i=5, GSI=15, D=0, and γ=25 kN/m^3. Considering different magnitudes of n, Fig. 9 shows the variation of the σ_p, which was obtained by optimizing Eq. (13). According to the results, the variation of σ_p is less than 1% for n>5. Thus, in this research, the optimal number of sliding blocks was considered equal to 5, and all the analyses in the following parts of this paper are based on n=5. It is worth noting that the same optimal number of sliding blocks was considered in the researches performed by Mollon *et al*. (2009a) and Zhao *et al*. (2017).

4. Results and discussions

4.1 Comparison with finite element method (FEM)

The results of the upper bound formulation developed in the present paper were compared with three-dimensional finite element models constructed using Plaxis 3D software. As shown in Fig. 10, only half of the tunnel geometry was modeled, given the symmetry of the problem. The model consisted of 77840 ten-nodded tetrahedral elements. The lower boundary of the model was constrained in the three main directions, while the lateral boundaries were free to move in the vertical direction. The distances between the tunnel and the side and bottom boundaries of the model were selected via trial and error so as not to affect the results. Since only determining the blow-out pressure was desired, not the convergence of the tunnel wall, the model was constructed without tunnel lining, and the tunnel walls have been fixed. Senet *et al.* (2013) were used the same approach for their models.

The numerical analyses involved 40 cases with the specifications shown in Table 1. The Hoek-Brown failure criterion was used for the rock mass, and no surcharge was considered on the top of the models. For each case, the deformation modulus and the Poisson's ratio of the rock mass were determined according to the recommendations of Hoek and Diederichs (2006) and Vásárhelyi (2009), respectively, as follows

Table 1 The parameters used

σ_{ci} (MPa)	1, 2.5, 5, 7.5, 10
GSI	10, 15, 20, 25
m_i	5, 10
D	0
γ (kN/m^3)	25
d (m)	10
C (m)	10

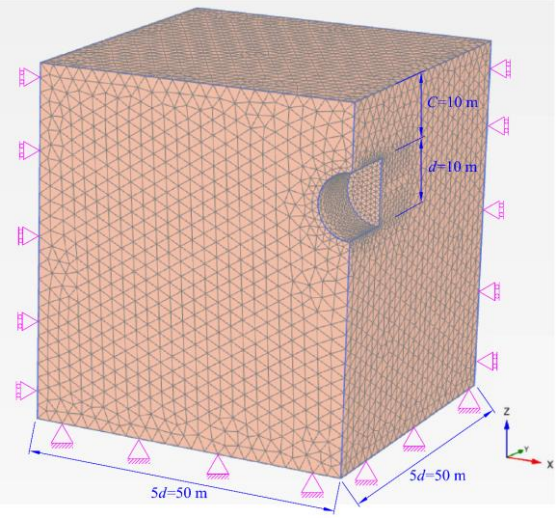

Fig. 10 Three-dimensional FEM model to calculate the blow-out pressure of the tunnel face

$$E_{rm}(MPa) = 100{,}000\left(\frac{1-D/2}{1+exp\left((75+25D-\mathrm{GSI})/11\right)}\right) \quad (25)$$

$$\nu_{rm} = -0.002\,\mathrm{GSI} - 0.003\,m_i + 0.457 \quad (26)$$

The bisection method used by Mollon et al. (2009b) and Senet *et al*. (2013) was applied to calculate the blow-out pressure from the FEM. In this method, arbitrary upper and lower bound pressures were applied to the tunnel face, for which the tunnel face was stable and unstable, respectively. In the finite element models, the instability was considered a condition where the analyses were not converged to a specific result. Then, by applying a pressure equal to the mean value of the assumed upper and lower bound pressures, the numerical analyses were repeated, and the stability of the tunnel face was examined. If the system was stable for this mean value of the pressure, the upper bound of the pressure was replaced by this mean value of pressure, but if the system did not reach equilibrium, the lower bound of the pressure was replaced by the mean pressure. The process was repeated until the difference between the upper and lower bounds of the pressure applied to the tunnel face became less than a specific tolerance, which was selected here as equal to 0.1 kPa. In this case, the final value of the intended upper bound of the face pressure was selected as the final blow-out pressure, which makes the tunnel face stable. This procedure was performed for all combinations of parameters presented in Table 1, and the corresponding

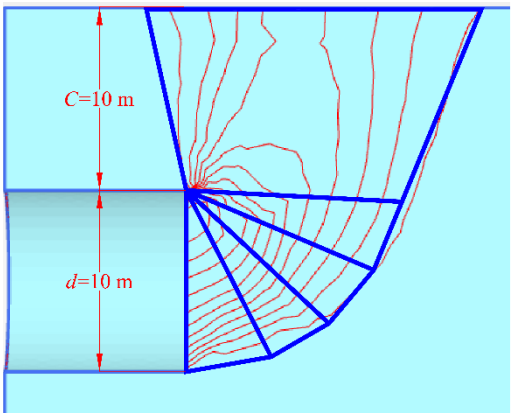

Fig. 11 Comparison of the total displacement contours obtained from FEM with the final scheme of the proposed failure mechanism for Case 2

σ_p was determined. Table 2 compares the σ_p obtained from the upper bound method (UBM) proposed in this paper and the finite element method (FEM). For all considered cases, the σ_p obtained from the UBM is 26.4% to 33.9% smaller than the FEM. Therefore, using the results of the presented upper bound formulation in practical applications is more conservative than the results of the FEM. Given the difficult and time-consuming nature of numerical modeling and the high skills required, using the upper bound technique presented in this research is appropriate for obtaining σ_p in the initial design phases of tunneling projects. For Case 2 of Table 2, Fig. 11 shows a 2D cross-section of the failure mechanism obtained from the presented UBM and the total displacement contour lines obtained from the FEM. Good agreement was observed between the results of the two methods.

4.2 Comparison with the available analytical and numerical methods

To the authors' knowledge, no analytical method is available regarding the blow-out pressure in rock masses, and the previously mentioned method proposed by Huang *et al.* (2018) only presents the final shape of the blow-out failure mechanism as a function of a specific value of the blow-out pressure. Hence, the UBM presented in this paper was compared with the analytical solutions available for the blow-out pressure in the soil medium. It should be noticed that the upper bound solution presented in this paper is based on the Hoek-Brown failure criterion, while the methods available for the blow-out pressure of soil medium are commonly based on the Mohr-Coulomb failure criterion. Therefore, a relationship must first be established between these two criteria to compare them together. This correlation was proposed by Hoek *et al*. (2002), and it is provided in RocLab program. Using this software, the Hoek-Brown parameters of a rock mass can be transformed to equivalent Mohr-Coulomb parameters from the following equations

$$\phi' = \sin^{-1}\left[\frac{6am_b(s+m_b\sigma'_{3n})^{a-1}}{2(1+a)(2+a)+6am_b(s+m_b\sigma'_{3n})^{a-1}}\right] \quad (27)$$

Table 2 A comparison of σ_p obtained from the UBM and FEM

Case	σ_{ci} (MPa)	GSI	σ_p (kPa) m_i=5 Present study			Case	σ_{ci} (MPa)	GSI	σ_p (kPa) m_i=10 Present study		
			UBM	FEM	Difference (%)				UBM	FEM	Difference (%)
1	1	10	1114.39	1516.2	-26.5	21	1	10	1348.71	1839.9	-26.7
2		15	1214.20	1790.5	-32.2	22		15	1526.82	2159.6	-29.3
3		20	1289.13	1935.6	-33.4	23		20	1682.88	2504.2	-32.8
4		25	1394.00	2108.9	-33.9	24		25	1883.76	2820.0	-33.2
5	2.5	10	1318.72	1796.6	-26.6	25	2.5	10	1865.98	2559.6	-27.1
6		15	1522.54	2082.8	-26.9	26		15	2263.94	3157.5	-28.3
7		20	1754.73	2481.9	-29.3	27		20	2699.16	3946.1	-31.6
8		25	2020.31	2945.1	-31.4	28		25	3181.49	4777.0	-33.4
9	5	10	1655.13	2248.8	-26.4	29	5	10	2709.75	3800.5	-28.7
10		15	2052.89	2843.3	-27.8	30		15	3480.90	4930.4	-29.4
11		20	2501.77	3553.7	-29.6	31		20	4362.38	6387.1	-31.7
12		25	3015.78	4481.1	-32.7	32		25	5,291.02	7980.4	-33.7
13	7.5	10	1971.99	2708.8	-27.2	33	7.5	10	3534.66	5020.8	-29.6
14		15	2561.23	3627.8	-29.4	34		15	4711.34	6788.7	-30.6
15		20	3244.90	4689.2	-30.8	35		20	6257.03	9297.2	-32.7
16		25	4020.46	5965.1	-32.6	36		25	7473.46	11137.8	-32.9
17	10	10	2297.54	3182.2	-27.8	37	10	10	4323.01	6166.9	-29.9
18		15	3043.85	4392.3	-30.7	38		15	6011.31	8762.8	-31.4
19		20	3987.63	5872.8	-32.1	39		20	8094.97	12046.1	-32.6
20		25	4966.52	7479.7	-33.6	40		25	9596.34	14495.9	-33.8

$$c' = \frac{\sigma_{ci}[(1+2a)s+(1-a)m_b\sigma'_{3n}](s+m_b\sigma'_{3n})^{a-1}}{(1+a)(2+a)\sqrt{1+(6am_b(s+m_b\sigma'_{3n})^{a-1})/((1+a)(2+a))}} \quad (28)$$

Where, $\sigma'_{3n}=\sigma'_{3max}/\sigma_{ci}$, and σ'_{3max} is the upper limit of confining stress.

For a tunnel with d=10 m, C=10 m, and σ_s=0, two sets of Hoek-Brown parameters were considered for the surrounding rock mass. The first set consisted of σ_{ci}=1 MPa, m_i=5, GSI=10, D=0, and γ=18 kN/m^3, and the second set is σ_{ci}=1 MPa, m_i=18, GSI=5, D=0 and γ=18 kN/m^3. The equivalent Mohr-Coulomb shear strength parameters of the first and second sets are (ϕ=17°, c=7 kPa) and (ϕ=25°, c=10 kPa), respectively. For these two sets of parameters, comparisons were conducted between the results of the proposed UBM and the analytical methods presented by other researchers for soil grounds. The results of these comparisons were presented in Tables 3 and 4, respectively. The comparison reveals that the σ_p obtained from the proposed UBM is smaller than those obtained from other methods, which is more valuable in the viewpoint of the upper bound theorem. The main reason for such a considerable difference is that in all the methods mentioned in Tables 3 and 4, a constant ϕ was assumed in the whole mechanism. However, in the present study, various ϕ_t values were considered through the failure mechanism. Moreover, the transformation of a Hoek-Brown rock mass to a Mohr-Coulomb soil arises discrepancies among the results. Figs. 12(a) and 12(b), 13(a) and 13(b) show 2D section and 3D view of the final failure mechanism for the two assumed Hoek-Brown parameter sets, respectively. Moreover, Figs. 12(c) and 13(c) display comparisons between the displacement contour lines resulting from the finite element analyses and the final shape of the proposed failure mechanism.

Table 3 Comparison of σ_p obtained from the proposed UBM with the existing methods (ϕ=17° and c=7 kPa)

Method	Approach	σ_p (kPa)	Difference with the presented UBM (%)
Present study	Upper bound solution	843.03	-
	Finite element	1265.4	-33.38
Leca & Dormieux (1990)	Limit analysis	1651.7	-49.0
Mollon *et al.* (2009a)	Limit analysis	1332.6	-36.7
Mollon *et al.* (2011a)	Limit analysis	1096.6	-23.1
Mollon *et al.* (2011a)	Finite difference	1113	-24.3
Zhao *et al.* (2017)	Limit analysis	1289.1	-34.6

The results of the present paper were also compared with the finite element limit analysis method applied by Shiau and Al-Asadi (2020). They considered a tunnel with C=12 m and d=6 m, constructed in a soil ground assuming ϕ=5°, c=27 kPa, γ=18 kN/m^3, and σ_s=0. The blow-out

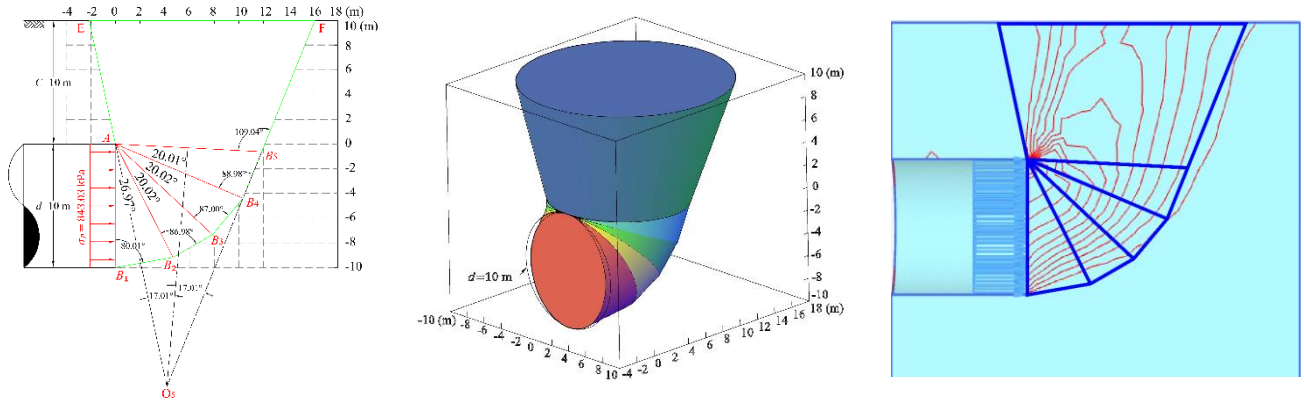

(a) (b) (c)

Fig. 12 The final shape of the proposed failure mechanism for ϕ=17º and c=7 kPa, (a) 2D section, (b) 3D view of the mechanism, and (c) displacement contour lines and the associated failure mechanism

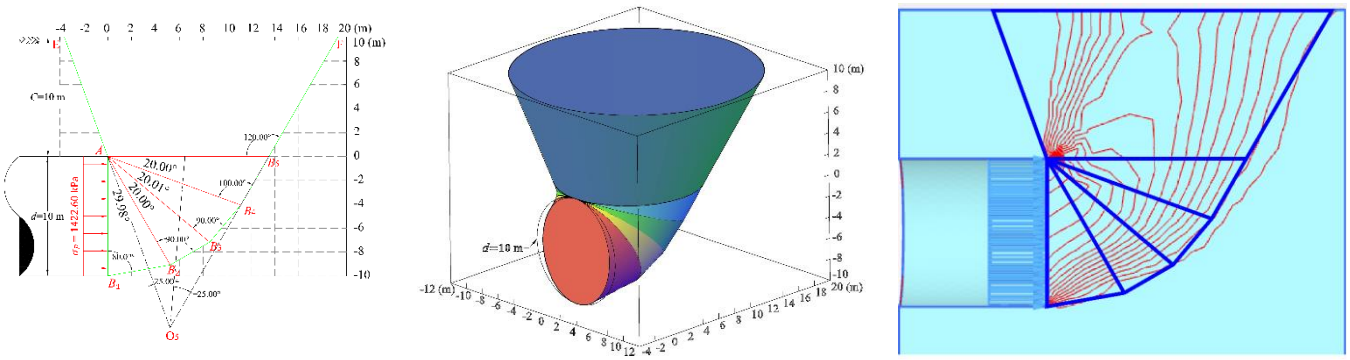

(a) (b) (c)

Fig. 13 The final shape of the proposed failure mechanism for ϕ=25º and c=10 kPa, (a) 2D section, (b) 3D view of the mechanism, and (c) displacement contour lines and the associated failure mechanism

Table 4 Comparison of σ_p obtained from the proposed UBM with the existing methods (ϕ=25º and c=10 kPa)

Method	Approach	σ_p (kPa)	Difference with the presented UBM (%)
Present study	Upper bound solution	1422.60	-
	Finite element	2134.6	-33.36
Leca & Dormieux (1990)	Limit analysis	3786.6	-62.4
Mollon *et al.* (2009a)	Limit analysis	2712.3	-47.6
Mollon *et al.* (2011a)	Limit analysis	1903.5	-25.3
Mollon *et al.* (2011a)	Finite difference	2004	-29.0
Zhao *et al.* (2017)	Limit analysis	2666.1	-46.6

pressure for such a case was obtained equal to 537.8 kPa. For being possible to compare this case with the upper bound solution proposed in the current study, the Hoek-Brown parameters must be selected in such a way that the equivalent Mohr-Coulomb parameters (ϕ and c) become equal to the values considered by Shiau and Al-Asadi (2020). Assuming Hoek-Brown parameters as σ_{ci}=5.9 MPa, m_i=1, GSI=5, and D=0, the equivalent ϕ=4.8º and c=26 kPa were obtained using the RocLab software, which are approximately equal to the assumption made by Shiau and Al-Asadi (2020). The blow-out pressure of such a rock mass was obtained equal to 466.5 kPa from the relationship presented in this paper, which indicates a 13.3% improvement (reduction) compared with the solution by Shiau and Al-Asadi (2020).

4.3 Comparison with the experimental methods

Reviewing literature indicates that no considerable experimental methods are available for obtaining blow-out pressure in rock masses. Hence, the results of the upper bound method presented in this study were compared with the physical 1 g tests performed by Berthoz *et al.* (2012). They considered a tunnel with d=0.55 m, and C=0.6 m excavated in homogeneous frictional soil assuming ϕ=36º, c=2.5 kPa, γ=13.20 kN/m^3, and σ_s=0. For such a case, the blow-out pressure was equal to 21 kPa. Berthoz *et al.* (2012) compared their results with the upper bound method proposed by Subrin (2002), which concluded a blow-out pressure equal to 612 kPa. Berthoz *et al*. (2012) attributed

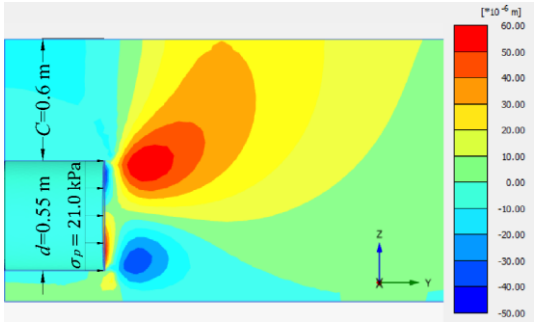

(a)

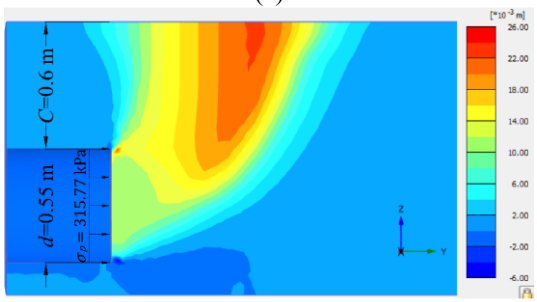

(b)

Fig. 14 Soil vertical displacement due to the face pressure obtained from the (a) Berthoz *et al.* (2012) with σ_p=21 kPa, and (b) the upper bound solution proposed in this study with σ_p =315.77 kPa

this large difference, i.e., 2814.29%, to the difference between the ground displacements before failure in these two methods. In other words, the blow-out pressure obtained from the experimental method, i.e., Berthoz *et al.* (2012) method, is equal to the pressure corresponding to the start of heaving in the ground surface, while in the upper bound method, i.e., Subrin (2002) method, it is equal to the pressure which results in a considerable increment in the plastic strains around the tunnel face leading to very large displacements ahead of the tunnel face and following by the development of the failure to the ground surface. It means that the criterion of the surface heave adopted by Berthoz *et al.* (2012) method is not suitable to evaluate blow-out pressure. For comparing these results with the upper bound solution presented in this paper, a rock mass with the Hoek-Brown parameters of σ_{ci}=0.035 MPa, m_i=10, GSI=55, and D=0 was considered. Using the RocLab program, the equivalent Mohr-Coulomb parameters were obtained as ϕ=36° and c=1.4 kPa, which are approximately similar to the values assumed by Berthoz *et al.* (2012). For such a rock mass, the upper bound formulation developed in the present study resulted in a blow-out pressure equal to 315.77 kPa, which is 1403.67% higher than the experimental value of Berthoz *et al.* (2012). The reason for such a high difference is the same as the points made to justify the difference between the results of Berthoz *et al.* (2012) and Subrin (2002). For explaining such a high difference between the empirical results of Berthoz *et al.* (2012) and those of the upper bound technique presented here, 3D finite element modeling was performed. To this end, two 3D finite element models were constructed. The first model was subjected to the tunnel face pressure recommended by Berthoz *et al.* (2012), i.e., 21 kPa, while the second one was subjected to that obtained from the upper bound solution proposed in this paper, i.e., 315.77 kPa. As shown in Fig. 14(a), the displacement of the ground surface right above the tunnel face was almost zero in the first model, while a surface heave of 5.8 mm was observed in the second model, as shown in Fig. 14(b), increasing to a maximum of 22.2 mm at a distance of 0.7 m in front of the tunnel face. Hence, the blow-out pressure obtained from the experimental method of Berthoz *et al.* (2012) corresponds to the onset of surface heave above the tunnel, while the blow-out pressure obtained from the upper bound method leads to a great surface heave.

It should be mentioned that for the considered case, the blow-out pressure obtained from the present research, i.e., 315.77 kPa, was 48.4% smaller than that obtained from the method by Subrin (2002), i.e., 612 kPa. This indicates that considering the upper bound method specifications, the technique presented here is more valuable than Subrin (2002).

5. Parametric analyses

Using the upper bound formulation presented in this paper, extensive parametric analyses were performed to investigate the effects of different parameters on the blow-out pressure. The following results were obtained.

5.1 Effect of tunnel diameter on σ_p

In order to examine the effect of tunnel diameter on σ_p, two rock masses with the parameters (σ_{ci}=1 MPa, m_i=5) and (σ_{ci}=2.5 MPa, m_i=10) were considered. For both cases, GSI=15 and D=0 were assumed. Moreover, two unit weights, namely 20 kN/m^3 and 25 kN/m^3 were considered for each case. The distance between the ground surface and the center of the tunnel was assumed equal to 15 m (C+d/2=15 m). Fig. 15 shows the variation of $\sigma_p/\gamma d$ versus d. As can be seen, the blow-out pressure decreases with an increase in the tunnel diameter. The rate of decrement reduces with an increase in the tunnel diameter. For the rock mass with σ_{ci}=1 MPa, m_i=5, and γ=20 kN/m^3, with

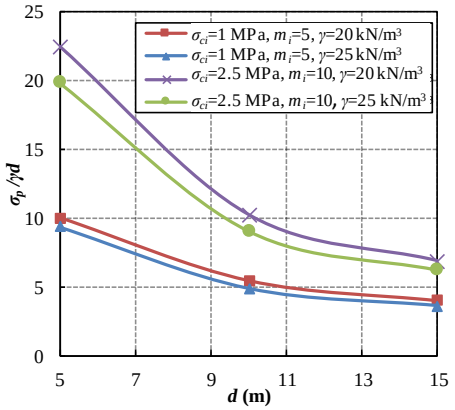

Fig. 15 Variation of $\sigma_p/\gamma d$ versus d

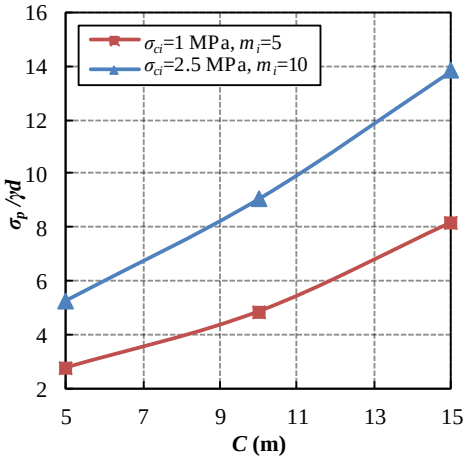

Fig. 16 Variation of $\sigma_p/\gamma d$ versus C

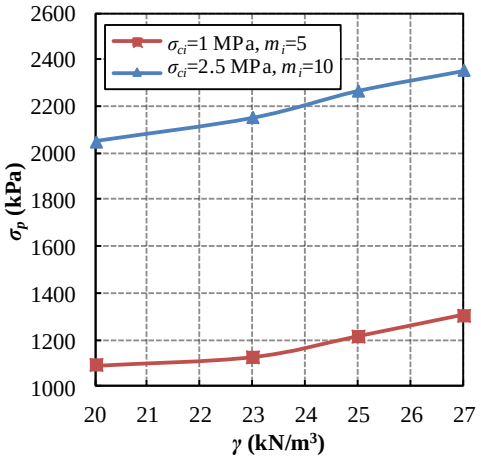

Fig. 17 Variation of σ_p versus γ

increasing the tunnel diameter from 5 m to 15 m, σ_p decreases by almost 59.8%. However, for the case of σ_{ci}=2.5 MPa, m_i=10, and γ=20 kN/m^3, which implies a stronger rock mass, this reduction is about 69.4%. Moreover, the obtained results show that for each set of the considered values of σ_{ci} and m_i, increasing γ results in decreasing σ_p at the maximum of 16.9%.

5.2 Effect of the height of the tunnel cover on σ_p

Considering two sets of rock mass properties, namely (σ_{ci}=1 MPa, m_i=5) and (σ_{ci}=2.5 MPa, m_i=10), Fig. 16 shows the variation of $\sigma_p/\gamma d$ versus the height of the tunnel cover (C). For both sets of the rock mass properties, it was assumed that GSI=15, D=0, γ=25 kN/m^3, and d=10 m. As can be seen, increasing the height of the tunnel cover leads to an increase in the σ_p. For every meter of increase in the height of the tunnel cover, the value of σ_p increases in the range of 26.2% to 29.4%.

5.3 Effect of the unit weight of the rock mass on σ_p

To investigate the effect of the unit weight of the rock mass on the blow-out pressure, two rock masses with the

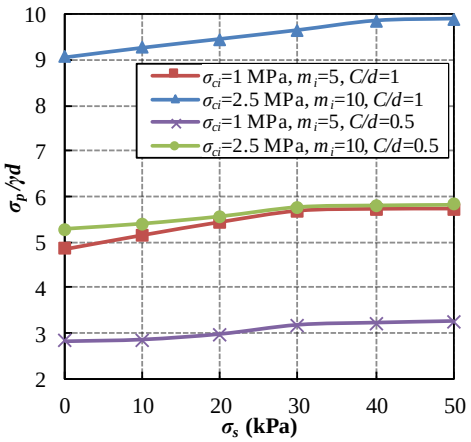

Fig. 18 Variation of $\sigma_p/\gamma d$ versus σ_s considering C/d=1 and 0.5

parameters (σ_{ci}=1 MPa, m_i=5) and (σ_{ci}=2.5 MPa, m_i=10) were considered. For both cases, GSI=15, D=0, d=10 m, and C/d=1 were assumed. Fig. 17 shows the variation of the blow-out pressure versus the unit weight of the rock mass. As can be seen, increasing the unit weight of the rock mass results in increasing the blow-out pressure with a higher rate of increment for the rock masses with larger unit weight. As the unit weight increases from 20 kN/m^3 to 27 kN/m^3, σ_p increases in the range of 14.9% to 19.6%.

5.4 Effect of the surcharge pressure applied to the ground surface on σ_p

The effect of the surcharge pressure applied to the ground surface (σ_s) on the blow-out pressure was studied by considering two rock masses with the parameters σ_{ci}=1 MPa, m_i=5, i.e., the weaker rock mass, and σ_{ci}=2.5 MPa, m_i=10, i.e., the stronger rock mass. For both cases, GSI=15, D=0, γ=25 kN/m^3, d=10 m, and C=10 m and 5 m were assumed. As shown in Fig. 18, increasing σ_s from zero to 50 kPa induces a maximum of 16.8% and 12.4% increase in the blow-out pressure for C/d=1 and C/d=0.5, respectively.

5.5 Design graphs

To facilitate using the results of the proposed upper bound solution in engineering practice, Fig. 19 shows the dimensionless blow-out pressure for circular tunnels with C/d=0.5 and 1. As can be seen, an improvement in the strength and quality of the rock mass (i.e., an increase in the parameters σ_{ci}, m_i, and GSI) results in increasing the blow-out pressure. The contribution of the parameters m_i and GSI in σ_p is more than that of σ_{ci}.

6. Conclusions

This paper introduced an upper bound solution to calculate the blow-out pressure of circular tunnels excavated in rock masses. The major results obtained in this research are as follows:

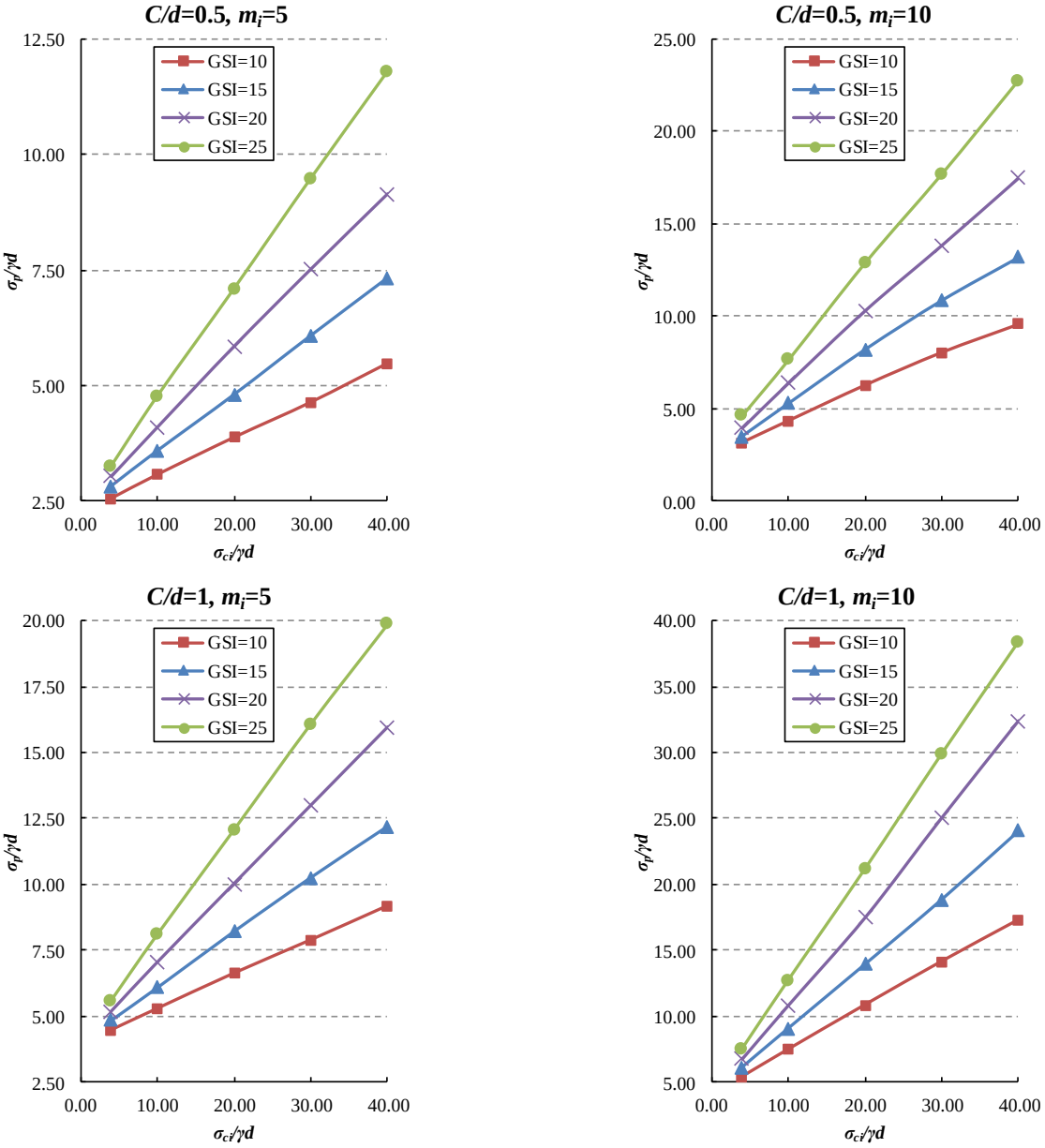

Fig. 19 Charts to determine the blow-out pressure considering C/d=0.5 and 1

- Most previous studies in the field of blow-out pressure consider constant values of ϕ and c in the whole mechanism. However, the main novelty of the proposed solution is to consider different values of ϕ_t and c_t through the failure mechanism. This contribution results in increasing the accuracy of the blow-out pressure.
- In all previous multi-block mechanisms, each sliding block was formed based on the geometry of its previous block. This geometry dependency was removed in the current study which results in more precise solutions.
- Increasing the strength parameters of the rock mass results in increasing the blow-out pressure. Among the studied rock mass properties, σ_{ci} and GSI have the largest and smallest effect on the blow-out pressure, respectively, while the effect of m_i lies somewhere between the effect of σ_{ci} and GSI.
- The obtained results show that the blow-out pressure increases almost linearly with an increase in σ_{ci}, the height of the tunnel cover, and the unit weight of the rock mass.
- Increasing the tunnel diameter results in decreasing the blow-out pressure. The rate of this reduction depends on σ_{ci}, m_i, and the unit weight of the rock mass.
- Increasing the surcharge pressure up to a certain level, results in increasing the blow-out pressure. Beyond this level, however, the blow-out pressure is not affected considerably by the surcharge pressure.
- The final shapes of the failure mechanism obtained from the proposed upper bound solution and the finite element modeling are well compatible. Using the

results of the proposed upper bound solution is much easier than three-dimensional finite element modeling of the blow-out pressure, especially in the initial design phases of engineering projects.

References

AlKhafaji, H., Imani, M. and Fahimifar, A. (2020), "Ultimate bearing capacity of rock mass foundations subjected to seepage forces using modified Hoek–Brown criterion", *Rock Mech. Rock Eng*., **53**, 251-268. https://doi.org/10.1007/s00603-019-01905-6.

Anagnostou, G. and Kovári, K. (1994), "The face stability of slurry-shield-driven tunnels", *Tunn. Undergr. Sp. Tech*., **9**(2), 165-174. https://doi.org/10.1016/0886-7798(94)90028-0.

Anagnostou, G. (2012), "The contribution of horizontal arching to tunnel face stability", *Geotechnik,* **35**(1), 34-44. https://doi.org/10.1002/gete.201100024.

Berthoz, N., Branque, D., Subrin, D., Wong, H. and Humbert, E. (2012)," Face failure in homogeneous and stratified soft ground: Theoretical and experimental approaches on 1g EPBS reduced scale model", *Tunn. Undergr. Sp. Tech.*, **30**, 25-37. https://doi.org/10.1016/j.tust.2012.01.005.

Bezuijen, A. and Brassinga, H.E. (2006), "Blow-out pressures measured in a centrifuge model and in the field", Tunnelling: a decade of progress: GeoDelft 1995-2005, *Taylor & Francis Group.*, London, Part 3, 143-148.

Broere, W. (2001), "Tunnel face stability and new CPT applications", PhD Thesis, Delf University Press., Delf, Netherlands.

Broms, B.B. and Bennermark, H. (1967), "Stability of clay at vertical openings", *J. Soil Mech. Found Eng.*, **193**(1), 71-94.

Chen, W.F. (1975), *Limit Analysis and Soil Plasticity*. Elsevier, Vol. **7**, Chapter 3, 47-106.

Davis, E.H., Gunn, M.J., Mair, R.J. and Seneviratne, H.N. (1980), "The stability of shallow tunnels and underground openings in cohesive material", *Géotechnique*, **30**(4), 397-416. https://doi.org/10.1680/geot.1980.30.4.397.

Guglielmetti, V., Grasso, P., Mahtab, A. and Xu, S. (2008), "Mechanized tunneling in urban areas: Design methodology and construction control", *Taylor and Francis Group*, Chapter 5, 113-235.

Han, K., Zhang, C. and Zhang, D. (2016), "Upper-bound solution for the face stability of a shield tunnel in multilayered cohesive-frictional soils", *Comput. Geotech.*, **79**, 1-9. https://doi.org/10.1016/j.compgeo.2016.05.018.

Herrenknecht, M. and Rehm, U. (2002), *Newest Development in Mechanized Tunneling*. Journées d'études Internationales, Toulouse, 201-206.

Hoek, E., Corranza-Torres, C.T. and Corkum, B. (2002), "Hoek-Brown failure criterion-2002 Edition", Proceedings of the *5th North American rock mechanics symposium*, Totonto, Canada.

Hoek, E. and Diederichs, M.S. (2006), "Emprical estimation of rock mass modulus", *Int. J. Rock Mech. Min. Sci.*, **43**(2), 203-215. https://doi.org/10.1016/j.ijrmms.2005.06.005.

Horn, M. (1961), "Horizontal earth pressure on perpendicular tunnel face", *Proceedings of the Hungarian National Conference of the Foundation Engineer Industry*, Budapest, Hungary, 7-16.

Huang, F., Qu, R., Li, Z., Yang, X. and Ling, T. (2018), "Limit analysis for the face stability of a shallow-shield tunnel based on a variational approach to the Blow-Out failure mode", *Int. J. Geomech*., **18**(6), 04018038. https://doi.org/10.1061/(ASCE)GM.1943-5622.0001150.

Huang, F., Feng, Y., Zhang, Z., Yang, X. and Ling, T. (2019), "Upper bound solution of the safety factor for a shield tunnel face subjected to the Hoek–Brown failure criterion", *Int. J. Civ. Eng.*, **17**, 1941-1950. https://doi.org/10.1007/s40999-019-00416-3.

Huang, F., Wang, D., Xiao, N. and Ou, R-C. (2021), "Upper bound limit analysis of blow-out failure mode of excavation face of shield tunnel considering groundwater seepage", *Geomech. Eng*., **26**(3), 227-234. https://doi.org/10.12989/gae.2021.26.3.227.

Imani, M. and Aali, R. (2020), "Effects of embedment depth of foundations on ultimate bearing capacity of rock masses", *Geotech. Geol. Eng.*, **38**, 6511-6528. https://doi.org/10.1007/s10706-020-01452-w.

Jancsecz, S. and Steiner, W. (1994), "Face support for a large mix-shield in heterogeneous ground conditions", *Tunn'94*, 531-550.

Khezri, N., Mohamad, H. and Fatahi, B. (2016), "Stability assessment of tunnel face in a layered soil using upper bound theorem of limit analysis", *Geomech. Eng*., **11**(4), 471-492. https://doi.org/10.12989/gae.2016.11.4.471.

Kirsch, A. (2009), "On the face stability of shallow tunnels in sand", *Advances in Geotechnical Engineering and Tunelling*, Logos, Berlin, Vol. **16**, 123.

Leca, E. and Dormieux, L. (1990), "Upper and lower bound solution for the face stability of shallow circular tunnels in frictional material", *Géotechnique*, **40**(4), 581-606. https://doi.org/10.1680/geot.1990.40.4.581.

Li, P., Chen, K., Wang, F. and Li, Z. (2019), "An upper-bound analytical model of blow-out for a shallow tunnel in sand considering the partial failure within the face", *Tunn. Undergr. Sp. Tech*., **91**, 102989. https://doi.org/10.1016/j.tust.2019.05.019.

Li, T.Z. and Yang, X.L. (2019), "Face stability analysis of rock tunnels under water table using Hoek-Brown failure criterion", *Geomech. Eng.*, **18**(3), 235-245. https://doi.org/10.12989/gae.2019.18.3.235.

Li, D., Zhao, L., Cheng, X. and Huang, F. (2020), "Active stability analysis of 3D shallow tunnel face with longitudinally inclined ground surface based on nonlinear Mohr–Coulomb failure criterion", *Int. J. Geomech*., **20**(11), 04020198. https://doi.org/10.1061/(ASCE)GM.1943-5622.0001844.

Li, D., Zhao, L., Cheng, X., Zuo, S. and Jiao, K. (2020), "Upper-bound limit analysis of passive failure of a 3D shallow tunnel face under the bidirectional inclined ground surfaces", *Comput. Geotech.*, **118**, 103310. https://doi.org/10.1016/j.compgeo.2019.103310.

Li, W., Zhang, C., Zhang, D., Ye, Z. and Tan, Z. (2022), "Face stability of shield tunnels considering a kinematically admissible velocity field of soil arching", *J. Rock Mech. Geotech. Eng*., **14**(2), 505-526. https://doi.org/10.1016/j.jrmge.2021.10.006.

Mair, R.J. and Taylor, R.N. (1997), "Bored tunneling in the urban environment", *Proceedings of the 14th International Conference on Soil Mechanics and Foundation Engineering*, Hamburg, Germany.

Mao, N., AL-Bittar, T. and Soubra, A.H. (2012), "Probabilistic analysis and design of strip foundation resting on rocks obeying Hoek-Brown failure criterion", *Int. J. Rock Mech. Min. Sci*., **49**, 45-58. https://doi.org/10.1016/j.ijrmms.2011.11.005.

Mollon, G., Dias, D. and Soubra, A.H. (2009a), "Probabilistic analysis and design of circular tunnels against face stability", *Int. J. Geomech*., **9**(6), 237-249. https://doi.org/10.1061/(ASCE)1532-3641(2009)9:6(237).

Mollon, G., Dias, D. and Soubra, A.H. (2009b), "Probabilistic analysis of circular tunnels in homogeneous soil using response surface methodology", *J. Geotech. Geoenviron. Eng*., **135**(9), 1314-1325. https://doi.org/10.1061/(ASCE)GT.1943-5606.0000060.

Mollon, G., Dias, D. and Soubra, A.H. (2010), "Face stability analysis of circular tunnels driven by a pressurized shield", *J. Geotech. Geoenviron. Eng.*, **136**(1), 215-229. https://doi.org/10.1061/(ASCE)GT.1943-5606.0000194.

Mollon, G., Dias, D. and Soubra, A.H. (2011a), "Rotational failure mechanisms for the face stability analysis of tunnels driven by pressurized shield", *Int. J. Numer. Anal. Methods Geomech.*, **35**(12), 1363-1388. https://doi.org/10.1002/nag.962.

Mollon, G., Phoon, K.K., Dias, D. and Soubra, A.H. (2011b), "Validation of a new 2D failure mechanism for the stability analysis of a pressurized tunnel face in a spatially varying sand", *J. Eng. Mech.*, **137**(1), 8-21. https://doi.org/10.1061/(ASCE)EM.1943-7889.0000196.

Mollon, G., Dias, D. and Soubra, A.H. (2013), "Continuous velocity fields of collapse and blowout of a pressurized tunnel face in purely cohesive soil", *Int. J. Numer. Anal. Methods Geomech.*, **37**(13), 2061-2083. https://doi.org/10.1002/nag.2121.

Murayama, S., Endo, M., Hashiba, T., Yamamoto, K. and Sasaki, H. (1966), "Geotechnical aspects for the excavating performance of the shield machines", *Proceedings of the 21st Annual Lecture in Meeting of Japan Society of Civil Engineers*, Tokyo, Japan.

Pan, Q. and Dias, D. (2017), "Upper-bound analysis on the face stability of a non-circular tunnel", *Tunn. Undergr. Sp. Tech.*, **62**, 96-102. https://doi.org/10.1016/j.tust.2016.11.010.

Pan, Q. and Dias, D. (2018), "Three-dimensional static and seismic stability analysis of a tunnel face driven in weak rock masses", *Int. J. Geomech.*, **18**(6), 1-10. https://doi.org/10.1061/(ASCE)GM.1943-5622.0001174.

Saada, Z., Maghous, S. and Garnier, D. (2008), "Bearing capacity of shallow foundations on rocks obeying a modified Hoek-Brown failure criterion", *Comput. Geotech.*, **35**(2), 144-154. https://doi.org/10.1016/j.compgeo.2007.06.003.

Saada, Z., Maghous, S. and Garnier, D. (2012), "Stability analysis of rock slopes subjected to seepage faces using the modified Hoek-Brown criterion", *Int. J. Rock Mech. Min. Sci.*, **55**, 45-54. https://doi.org/10.1016/j.ijrmms.2012.06.010.

Seghateh Mojtahedi, A., Imani, M. and Fahimifar, A. (2021), "Three-dimensional face stability analysis of deep and shallow tunnels in rock masses", *Int. J. Geomech.*, **21**(10), 04021193. https://doi.org/10.1061/(ASCE)GM.1943-5622.0002152.

Senet, S., Mollon, G. and Jimenez, R. (2013), "Tunnel face stability in heavily fractured rock masses that follow the Hoek-Brown failure criterion", *Int. J. Rock Mech. Min. Sci.*, **60**, 440-451. https://doi.org/10.1016/j.ijrmms.2013.01.004.

Shamloo, S. and Imani, M. (2021), "Upper bound solution for the bearing capacity of two adjacent footings on rock masses", *Comput. Geotech.*, **129**, 103855. https://doi.org/10.1016/j.compgeo.2020.103855.

Shiau, J. and Al-Asadi, F. (2020), "Three-dimensional heading stability of twin circular tunnels", *Geotech. Geol. Eng.*, **38**, 2973-2988. https://doi.org/10.1007/s10706-020-01201-z.

Sloan, S.W. and Assadi, A. (1994), "Undrained stability of a plane strain heading", *Can. Geotech. J.*, **31**, 443-450. https://doi.org/10.1139/t94-051.

Subrin, D. (2002), "Etudes théoriques sur la stabilité et le comportement des tunnels renforcés par boulonnage", These de doctorat soutenue à l'Institut National des Sciences Appliquées de Lyon, France.

Vásárhelyi, B. (2009), "A possible method for estimating the Poission's rate values of the rock masses", *Acta Geod. Geophys. Hung.*, **44**(3), 312-322. https://doi.org/10.1556/ageod.44.2009.3.4.

Vermeer, P.A., Ruse, N. and Marcher, T. (2002), "Tunnel heading stability in drained ground", *Felsbau*, **20**(6), 8-18.

Wong, K.S., Ng, C.W.W., Chen, Y.M. and Bian, X.C. (2012), "Centrifuge and numerical investigation of passive failure of tunnel face in sand", *Tunn. Undergr. Sp. Tech.*, **28**, 297-303. https://doi.org/10.1016/j.tust.2011.12.004.

Yang, X., Yang, Z., Hou, G., Jiang, Y., Shao, X. and Qi, W. (2022), "Evaluation of the active limit support pressure for shield tunnel face in clay–sand interface mixed ground", *Int. J. Geomech.*, **22**(7). https://doi.org/10.1061/(ASCE)GM.1943-5622.0002404.

Yang, X.L. and Yin, J.H. (2005), "Upper bound solution for ultimate bearing capacity with a modified Hoek-Brown failure criterion", *Int. J. Rock Mech. Min. Sci.*, **42**, 550-560. https://doi.org/10.1016/j.ijrmms.2005.03.002.

Zamora Hernández, Y., Durand Farfán, A. and Pacheco de Assis, A. (2019), "Three-dimensional analysis of excavation face stability of shallow tunnels", *Tunn. Undergr. Sp. Tech.*, **92**, 103062. https://doi.org/10.1016/j.tust.2019.103062.

Zhang, C., Han, K. and Zhang, D. (2015), "Face stability analysis of shallow circular tunnels in cohesive-frictional soils", *Tunn. Undergr. Sp. Tech.*, **50**, 345-357. https://doi.org/10.1016/j.tust.2015.08.007.

Zhao, L., Li, D., Li, L., Yang, F., Cheng, X. and Lou, W. (2017), "Three-dimensional stability analysis of a longitudinally inclined shallow tunnel face", *Comput. Geotech.*, **87**, 32-48. https://doi.org/10.1016/j.compgeo.2017.01.015.

Zou, J., Chen, G. and Qian, Z. (2019), "Tunnel face stability in cohesion-frictional soils considering the soil arching effect by improved failure models", *Comput. Geotech.*, **106**, 1-17. https://doi.org/10.1016/j.compgeo.2018.10.014.

CC

Appendix: The relationships associated with the failure mechanism proposed in this paper

Considering n sliding blocks in Fig. 5, the computations corresponding to the proposed failure mechanism are as follows

$$AB_1 = d \tag{A1}$$

$$AB_i = \frac{\sin\beta_{i-1}}{\sin(\alpha_{i-1}+\beta_{i-1})} AB_{i-1} \quad (i = 2,3,\dots,n) \tag{A2}$$

$$\theta_i = \frac{\pi}{2} - \beta_i + \phi_i \qquad (i = 1,2,\dots,n) \tag{A3}$$

$$h_i = AO_i \cdot \sin(\beta_i - 2\phi_i) = AB_i \cdot \frac{\sin\beta_i}{\sin 2\emptyset_i} \cdot \sin(\beta_i - 2\phi_i) \qquad (i = 1,2,\dots,n) \tag{A4}$$

$$\psi_1 = \beta_1 - \phi_1 \tag{A5}$$

$$\psi_i = \beta_i - \sum_{j=1}^{i-1} \alpha_j - \phi_i \quad (i = 2,3,\dots,n) \tag{A6}$$

According to Fig. 4, θ_i is the angle between the axis of the i^{th} cone and the perpendicular bisector of Plane 1. Also, h_i is the height, and α_i and β_i are the geometric angles of the i^{th} cone.

Absolute and relative velocity vectors:

According to Fig. 6(b) and using the law of sines, the magnitude of the absolute velocity of each sliding block and the relative velocity between two adjacent sliding blocks are as follows

$$U_{i+1} = \frac{\sin(\beta_{i+1} - \phi_i + \phi_{i,i+1})}{\sin(\alpha_i + \beta_i - 2\phi_i + \phi_{i+1} + \phi_{i,i+1})} U_i \ (i = 1,2,\dots,n-1) \tag{A7}$$

$$U_{i,i+1} = U_{r(i)} = \frac{\sin(\alpha_i + \beta_i - \beta_{i+1} - \phi_i + \phi_{i+1})}{\sin(\alpha_i + \beta_i - 2\phi_i + \phi_{i+1} + \phi_{i,i+1})} U_i \ (i = 1,2,\dots,n \tag{A8}$$

Volumes of the 1st to (n-1)th sliding blocks

As shown in Fig. 4

$$a_i = \frac{AB_i}{2} \qquad (i = 1,2,\dots,n) \tag{A9}$$

$$b_i = a_i \cdot \sqrt{1 - \left(\frac{\sin\theta_i}{\cos\phi_i}\right)^2} \quad (i = 1,2,\dots,n) \tag{A10}$$

$$A_i = \pi a_i b_i \qquad (i = 1,2,\dots,n) \tag{A11}$$

where a_i and b_i are half of the major and minor diameters, respectively, and A_i is the area of the i^{th} ellipse.

Given Fig. 7(b), the equation of the elliptical shape cross-section of the $(i+1)^{th}$ cone is as follows

$$y_{i+1} = \frac{b_{i+1}}{a_{i+1}} \sqrt{a_{i+1}^2 - (x_{i+1} - a_{i+1})^2} \ (i = 1,2,\dots,n-1) \tag{A12}$$

Using the law of sines

$$x_i = \frac{\sin(\alpha_i+\beta_i)}{\sin\beta_i} x_{i+1} = k_i x_{i+1} \ (i = 1,2,\dots,n-1) \tag{A13}$$

Hence, the equation of the elliptical shape cross-section of the i^{th} cone is as follows

$$y_i = \frac{b_i}{a_i} \sqrt{a_i^2 - (\frac{\sin(\alpha_i+\beta_i)}{\sin\beta_i} x_{i+1} - a_i)^2} \ (i = 1,2,\dots,n-1) \tag{A14}$$

Therefore, the angle δ_i, shown in Fig. 7(b), is as follows

$$\delta_i = \tan^{-1}\left(\frac{\frac{b_{i+1}}{a_{i+1}}\sqrt{a_{i+1}^2 - (x_{i+1} - a_{i+1})^2} - \frac{b_i}{a_i}\sqrt{a_i^2 - \left(\frac{\sin(\alpha_i+\beta_i)}{\sin\beta_i} x_{i+1} - a_i\right)^2}}{x_{i+1} \cdot \frac{\sin\alpha_i}{\sin\beta_i}} \right) \tag{A15}$$

$$(i = 1,2,\dots,n-1)$$

The volume of the differential element v_i with the base of *efgh* and the thickness Δx_{i+1}, shown in Fig. 7(b), was obtained as follows

$$v_i = \frac{2y_{i+1} + 2y_i}{2} x_{i+1} \frac{\sin\alpha_i}{\sin\beta_i} \Delta x_{i+1} \sin(\alpha_i + \beta_i) \qquad (i = 1,2,\dots,n-1) \tag{A16}$$

In order to calculate the volume of each sliding block V_i, one must integrate Eq. (A16) over the range of 0 to $2a_{i+1}$.

Hence

$$\begin{aligned} V_i &= \int_0^{2a_{i+1}} v_i \, dx_{i+1} \\ &= \int_0^{2a_{i+1}} \left(\frac{b_{i+1}}{a_{i+1}} \sin(\alpha_i + \beta_i) \frac{\sin\alpha_i}{\sin\beta_i} x_{i+1} \sqrt{a_{i+1}^2 - (x_{i+1} - a_{i+1})^2} \right. \\ &\left. + \frac{b_i}{a_i} \sin(\alpha_i + \beta_i) \frac{\sin\alpha_i}{\sin\beta_i} x_{i+1} \sqrt{a_i^2 - \left(\frac{\sin(\alpha_i+\beta_i)}{\sin\beta_i} x_{i+1} - a_i\right)^2} \right) dx_{i+1} \end{aligned} \tag{A17}$$

$$(i = 1,2,\dots,n-1)$$

By solving the definite integral of Eq. (A17), one can obtain the volume of the i^{th} sliding block as follows

$$\begin{aligned} V_i = \frac{b_{i+1}}{a_{i+1}} \sin(\alpha_i + \beta_i) \frac{\sin\alpha_i}{\sin\beta_i} \frac{\pi a_{i+1}^3}{2} + \frac{b_i}{a_i} \sin(\alpha_i + \beta_i) \frac{\sin\alpha_i}{\sin\beta_i} \frac{a_i^3}{{k_i}^2} \Big[\frac{1}{2} \\ \cdot \sin^{-1}\left(\frac{2a_{i+1}k_i - a_i}{a_i}\right) + \frac{\pi}{4} \\ + \frac{1}{4}\sin\left(2\sin^{-1}\left(\frac{2a_{i+1}k_i - a_i}{a_i}\right)\right) \\ - \frac{1}{3}\cos^3\left(\sin^{-1}\left(\frac{2a_{i+1}k_i - a_i}{a_i}\right)\right)\Big] \quad (i \\ = 1,2,\dots,n-1) \end{aligned} \tag{A18}$$

The lateral surface area of the 1st to (n-1)th sliding blocks

According to Fig. 8(b), the lateral surface area between the two elliptical bases was determined by integrating the surface differential element ds_{ai} with a length of l (or $\overline{gf}$) and a width of Δx_{i+1} over the range of 0 to $2a_{i+1}$. Given the equations of the $(i+1)^{th}$ and i^{th} ellipses (Eqs. (A12) and (A14), respectively) and using the mathematical expression for the length of a curve with an arbitrary equation, the lateral surface area of the 1st to $(n-1)^{th}$ sliding blocks is as follows

$$S_i = 2\int_0^{2a_{i+1}} ds_{ai}\cdot dx_{i+1} = 2\int_0^{2a_{i+1}} [l\cdot ds_{i+1}]\,dx_{i+1} = 2\int_0^{2a_{i+1}} \left[\sqrt{(y_{i+1}-y_i)^2+\left(\frac{\sin\alpha_i}{\sin\beta_i}x_{i+1}\right)^2}\cdot \sqrt{1+\left(\frac{-b_i k_i(k_i x_{i+1}-a_i)}{a_i\sqrt{a_i^2-(k_i x_{i+1}-a_i)^2}}\right)^2}\right] k_i\,dx_{i+1} \quad (i=1,2,\dots,n-1) \tag{A19}$$

where ds_i is the length of the elliptical curve of the i^{th} cone.

The dissipated internal energy required for upper bound calculations is equal to the project of each velocity vector on its corresponding surface, multiply by the area of that surface. According to Fig. 8(a), the angle between the velocity vector U_i and the lateral surface S_i is not constant. Hence, the projection of U_i onto every surface element ds_{ai} is included in the integration for S_i. Therefore, the final equation of the lateral surface area of the i^{th} to $(n\text{-}1)^{\text{th}}$ sliding blocks is as follows

$$S_i\cdot\int_0^{2a_{i+1}}\cos\delta_i\,dx_{i+1} = 2\int_0^{2a_{i+1}} ds_{ai}\cdot dx_{i+1}\cdot\int_0^{2a_{i+1}}\cos\delta_i\,dx_{i+1} = 2\int_0^{2a_{i+1}}\left[\left(\sqrt{(y_{i+1}-y_i)^2+\left(\frac{\sin\alpha_i}{\sin\beta_i}x_{i+1}\right)^2}\cdot\sqrt{1+\left(\frac{-b_i k_i(k_i x_{i+1}-a_i)}{a_i\sqrt{a_i^2-(k_i x_{i+1}-a_i)^2}}\right)^2}\right)k_i \cdot\cos\left(\tan^{-1}\left(\frac{\frac{b_{i+1}}{a_{i+1}}\sqrt{a_{i+1}^2-(x_{i+1}-a_{i+1})^2}-\frac{b_i}{a_i}\sqrt{a_i^2-(k_i x_{i+1}-a_i)^2}}{x_{i+1}\frac{\sin\alpha_i}{\sin\beta_i}}\right)\right)\right]dx_{i+1} \tag{A20}$$

where the angle δ_i was shown in Fig. 8(b).

Eq. (A20) is a complicated nonlinear integral that is difficult to solve. To facilitate solving this integral, the Gaussian Quadrature integration technique was employed.

The volume and surface area of the n^{th} sliding block

The n^{th} sliding block, i.e., the block touching the ground surface, is a truncated cone which the vertical distance between its vertex and the ground surface is as follows

$$h_{n+1} = AO_n\cdot\sin\left(\frac{\pi}{2}+\beta_n-\sum_{i=1}^{n-1}\alpha_i-2\phi_n\right)+C = AB_n\cdot\frac{\sin\beta_n}{\sin 2\phi_n}\cdot\sin\left(\frac{\pi}{2}+\beta_n-\sum_{i=1}^{n-1}\alpha_i-2\phi_n\right)+C \tag{A21}$$

Moreover, as shown in Fig. 5, the length of the sides and various other geometric parameters of this truncated cone are as follows

$$AE = \frac{C}{\sin\left(\frac{\pi}{2}+\beta_n-\sum_{i=1}^{n-1}\alpha_i-2\phi_n\right)} \tag{A22}$$

$$EO_n = AO_n + AE \tag{A23}$$

$$EF = \frac{EO_n\cdot\sin(2\phi_n)}{\sin\left(\frac{\pi}{2}-\beta_n+\sum_{i=1}^{n-1}\alpha_i\right)} \tag{A24}$$

$$a_{n+1} = \frac{EF}{2} \tag{A25}$$

$$\theta_{n+1} = \phi_n - \beta_n + \sum_{i=1}^{n-1}\alpha_i \tag{A26}$$

$$b_{n+1} = a_{n+1}\sqrt{1-\left(\frac{\sin\theta_{n+1}}{\cos\phi_n}\right)^2} \tag{A27}$$

$$A_{n+1} = \pi a_{n+1} b_{n+1} \tag{A28}$$

where θ_{n+1} is the angle between the axis of the truncated cone and the vertical direction. The volume and the lateral surface area of the cone EO_nF in Fig. 5 are as follows

$$V_{n+1} = \frac{1}{3}A_{n+1}h_{n+1} \tag{A29}$$

$$S_{n+1} = A_{n+1}\frac{\cos\theta_{n+1}}{\sin\phi_n} \tag{A30}$$

Hence, one can obtain the final equations for the volume and lateral surface area of the truncated cone $AEFB_n$ by subtracting the above values from the volume and the lateral surface area of the cone EO_nF, as follows

$$V_{TC} = V_{n+1} - V_n = \frac{1}{3}(A_{n+1}h_{n+1} - A_n h_n) \tag{A31}$$

$$S_{TC} = S_{n+1} - S_n = A_{n+1}\frac{\cos\theta_{n+1}}{\sin\phi_n} - A_n\frac{\cos\theta_n}{\sin\phi_n} \tag{A32}$$

List of symbols

The following symbols are used in this paper:

A_i and A_{i+1} = The base area of the i^{th} and $(i+1)^{th}$ elliptical cones;
C = The height of the tunnel cover;
c_i and $c_{i,\ i+1}$ = Tangential cohesions corresponding to ϕ_i and $\phi_{i,\ i+1}$, respectively;
c_t = Tangential cohesion corresponding to ϕ_t;
D = Disturbance coefficient;
d = The diameter of the tunnel;
FEM = Finite Element Method;
FDM = Finite Difference Method;
GSI = Geological strength index of rock masses;
h_i = The height of i^{th} cone;
m_b = Value of the Hoek-Brown constant, m for rock masses;
m_i = Value of m for intact rocks;
n = Number of sliding blocks;
s and a = Hoek-Brown constants which depend upon the characteristics of rock masses;
S_i = The lateral area of the i^{th} sliding block;
UBM = Upper Bound Method;
U_i = The absolute velocity of the i^{th} sliding blocks;
$U_{r(i)}$ or $U_{i,\ i+1}$ = The relative velocity between the i^{th} and $(i+1)^{th}$ sliding blocks;
V_i = The volume of the i^{th} sliding block;
ϕ_i = Tangential friction angle along the lateral surface of the i^{th} elliptical cone;
$\phi_{i,\ i+1}$ = Relative tangential friction angle between the i^{th} and $(i+1)^{th}$ sliding blocks;
ϕ_t = Tangential friction angle;
γ = The unit weight of rock masses;
σ'_1 and σ'_3 = The major and minor effective principal stresses at failure, respectively;
σ_{ci} = Uniaxial compressive strength of intact rocks;
σ_p = The tunnel face pressure;
σ_s = The surcharge pressure applied to the ground surface;
ψ_i = The angle between the absolute velocity of the i^{th} sliding block and the vertical direction;